Crack-tip shielding in silica at room temperature

K.G. Schell, T. Fett, C. Bucharsky
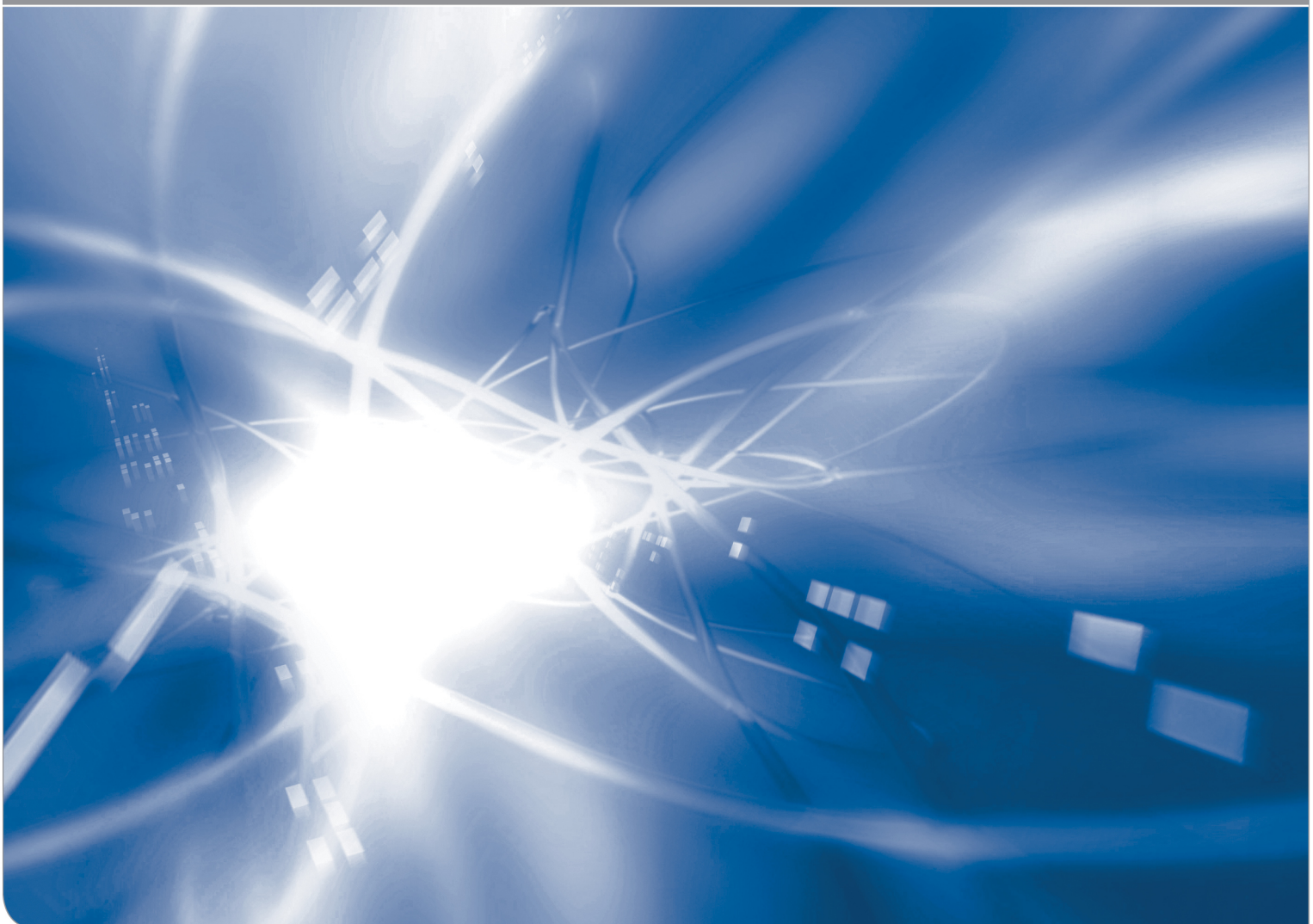
IAM Institute for Applied Materials

Abstract

When water penetrates into silica surfaces near a crack tip, it reacts with the SiO_2 network and generates hydroxyl $\equiv$SiOH. Due to the hydroxyl generation, the glass must expand. Since a free expansion is not possible for the thin layers on the undeformed bulk material, compressive stresses occur which shield the crack-tip region from externally applied tensile load. The consequence is a fracture mechanics shielding stress intensity factor $K_{sh}<0$.

So far we only determined the shielding stress intensity factor from theoretical considerations on water diffusion und the high tensile stresses at crack tips. Since water concentration measurements on crack surfaces of uncritically driven cracks are available in literature, we determine the shielding term K_{sh} from experimental data. This evaluation is done with and without consideration of damaging the initial ring network by hydroxyl generation.

It can be concluded that the shielding stress intensity factor is clearly overestimated, when crack-tip damage is ignored. Finally, it is illustrated in which way the shielding stress intensity factor influences the *v*-*K*-curve for subcritical crack growth.

Contents

1. Introduction

The reaction of water and silica in the surface diffusion zone affects the fracture mechanics stress intensity factor K at the tips of cracks. At temperatures $T < 500°C$, the equilibrium constant of the water/silica-reaction

$$\equiv\text{Si-O-Si}\equiv +H_2O \leftrightarrow \equiv\text{SiOH+HOSi}\equiv \tag{1}$$

is given by

$$k_1 = \frac{S}{C}. \tag{2}$$

where, $S=[\equiv\text{SiOH}]$, is the concentration of the hydroxyl groups in the silica network and $C=[H_2O]$ the concentration of unreacted water.
According to Le Chatelier [1], the equation governing the equilibrium constant is

$$\frac{\partial \ln k_1}{\partial p} = -\frac{\Delta\overline{V}}{RT}. \tag{3}$$

where p is pressure, $\Delta\overline{V}$ is the reaction volume, R the universal gas constant, and T the temperature in °K. By replacing the hydrostatic pressure p by the hydrostatic stress σ_h in a solid

$$\sigma_h = \tfrac{1}{3}(\sigma_x + \sigma_y + \sigma_z) \tag{4}$$

we obtain with the hydroxyl concentration S_0 for $\sigma_h=0$

$$S = S_0 \exp\left(\frac{\sigma_h\Delta\overline{V}}{RT}\right) \quad , \quad \sigma_h = -p \tag{5}$$

This relation implies that in the high crack-tip stress field nearly all water C_w is present in form of hydroxyl S. As could be deduced from density measurements reported in [2], hydroxyl generation results in a volume expansion ε_v

$$\varepsilon_v = \kappa \times S \tag{6}$$

with $\kappa\cong0.97$ derived from density measurements on specimens with small water concentrations reported by Shelby [2].
For a crack of depth a, the singular hydrostatic near-tip stresses are given as

$$\sigma_h = \tfrac{2}{3}(1+\nu)\frac{K}{\sqrt{2\pi r}}\cos(\varphi/2) \tag{7}$$

where r and φ are the polar coordinates with the origin at the crack tip. As a consequence of eq.(5), very high hydroxyl concentrations and swelling strains must occur in

the crack-tip region. This allows the assumption that near a crack tip the water is present predominantly in the form of hydroxyl water.

2. Effect of local swelling at surface cracks

2.1 Shielding zone at a crack tip

Due to restrictions in free expansion, the swelling strains ε_v result in swelling stresses which give rise for the "shielding" stress intensity factor $K_{sh}<0$. At first loading, the swelling zone at the crack tip $r(\sigma_h,\varphi)$ is heart-shaped as illustrated in Fig. 1a.
The height of the contour for constant hydrostatic stress σ_h is due to eq.(7)

$$\omega = \frac{(1+\nu)^2}{4\sqrt{3}\pi}\left(\frac{K_I}{\sigma_h}\right)^2 \tag{8}$$
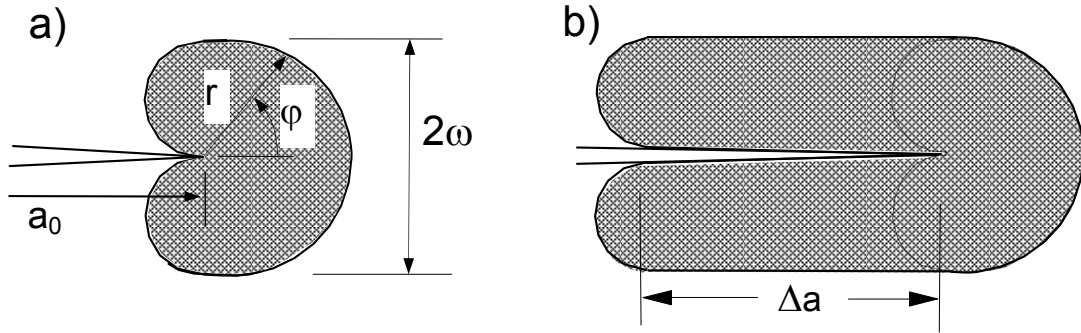
Fig. 1 a) Swelling zone at the tip of an arrested crack under mechanical loading, caused by stress-enhanced diffusion, b) zone for a crack grown by Δa.

The shielding stress intensity factor caused by a swelling zone of height ω is [3]

$$K_{sh} = -\psi\frac{\varepsilon_v E}{1-\nu}\sqrt{\omega} \tag{9}$$

where E is Young's modulus and ν Poisson's ratio. The zone of an arrested crack (not grown before loading) is heart-shaped, Fig. 1a, resulting in the coefficient **ψ=0**. When a crack has grown at least for $\Delta a \cong 5\omega$, Fig. 1b, a value of **ψ=0.22** is reached as was shown by McMeeking and Evans [3] and confirmed in [4]. The coefficient ψ was computed in [3] also for different shapes at the zone end as illustrated in Fig. 2a. Fig. b shows the related coefficients ψ for the general representation by eq.(9) as the solid circles. We interpolate these data by the interpolating curve through the data points that can be expressed simply by

$$\psi \cong 0.37\left(1 - \tfrac{1}{2}\tanh\left(\frac{7}{9}\frac{r_0}{\omega}\right)\right) \qquad (10)$$

As an application of this relation, the coefficient ψ may be estimated for a deviating zone shape. Computations of swelling zones are mostly carried out for diffusion in a motionless coordinate system with a fixed crack tip, i.e. for an *arrested* crack. Whereas for a *growing* crack the transversal diffusion normal to the crack plane is hardly affected by the moving crack tip, the diffusion and the crack propagation compete in crack direction [5,6]. In [7] it was found for crack rates $v>10^{-12}$ m/s under the assumption that the diffusion normal to the crack-plane direction is not affected by the crack rate ($v_\perp = 0$)

$$\tfrac{3}{4}\frac{8}{\sqrt{27}} < \frac{r_0}{\omega} < \frac{8}{\sqrt{27}} \qquad (11)$$

For $r_0/\omega = 0.8 \times 8/\sqrt{27} \cong 1.23$, it results from eq.(10) $\psi \cong 0.23$, introduced in Fig. 2b as the open circle.
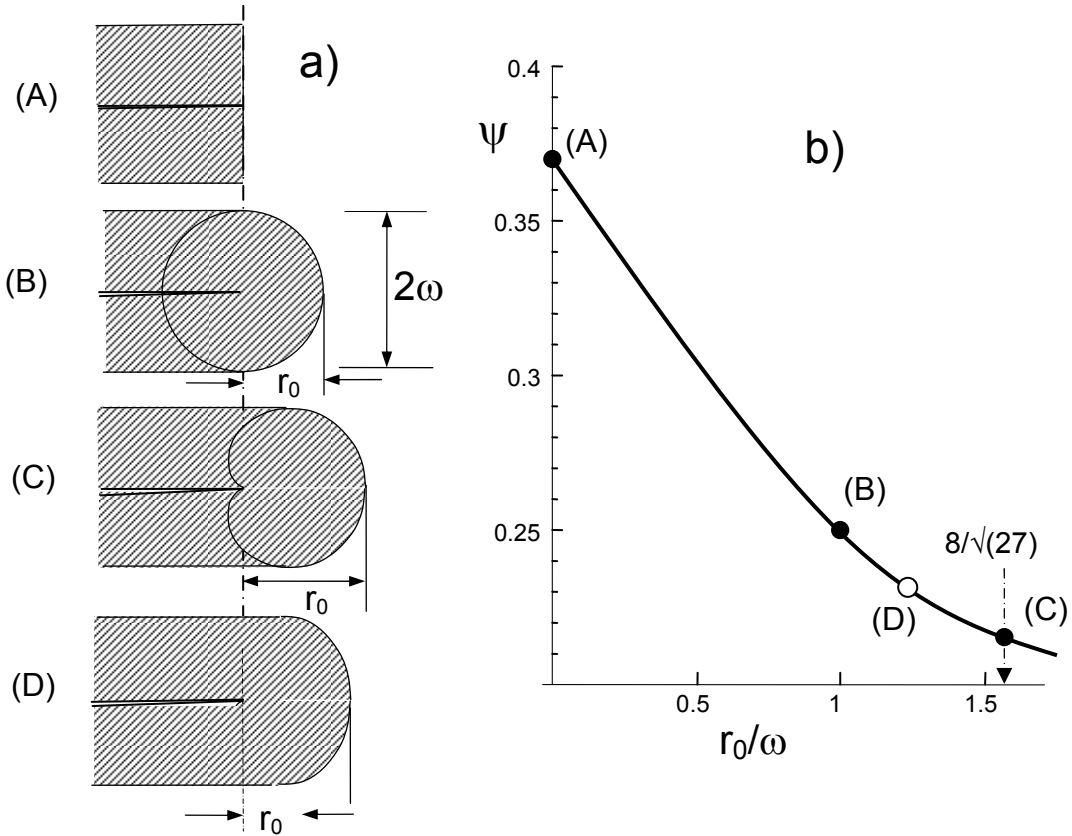
Fig. 2 Cracks grown for $\Delta a > 5\omega$, a) swelling zones with different shape at the zone end, b) shielding stress intensity factors by eq.(9) (circles) and interpolating curve according to eq.(10) for the zone ends given in a), open circle represents the case of a growing crack with competing rates of crack rate and diffusion, case (D).

2.2 Shielding stress intensity factor for varying hydroxyl concentration

In Section 2.1 we considered zones with constant swelling volume ε_v. In the general case, we have to expect hydroxyl concentrations and swelling strains that decrease with distance from the crack. A Green's function procedure for such cases had been developed in [8].

Equation (9) holds for the case of a step-shaped constant strain $\varepsilon = \varepsilon_0$ inside and $\varepsilon = 0$ outside the swelling zone. For the more general case, we have to subdivide the zone in parts of thickness $d\omega'$ at a distance, ω', from the crack plane (Fig. 3).

The stress intensity factor caused by this zone of strain $\varepsilon(\omega')$ results from (9) as

$$d(K_{sh}) = -\tfrac{1}{2} 0.22 \frac{\varepsilon_v E}{1-v} \frac{1}{\sqrt{\omega'}} d\omega' \tag{12}$$

Now the stress intensity factor for the varying ε_v results from

$$K_{sh} = \int_0^\infty \varepsilon_v \, h(\omega') \, d\omega' \tag{13}$$

with the Green's- or "weight function" h

$$h \stackrel{def}{=} -0.11 \frac{E}{1-v} \frac{1}{\sqrt{\omega'}} \tag{14}$$
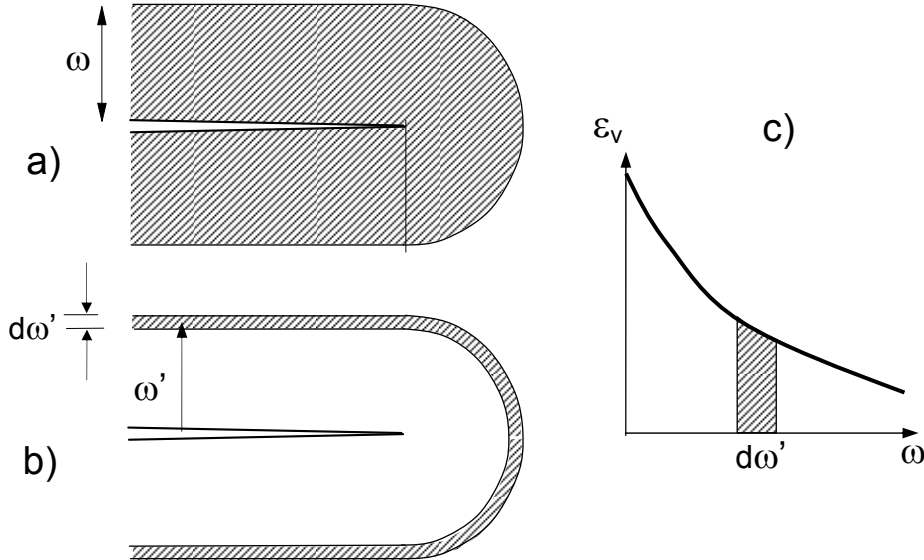
Fig. 3 a) Zone with constant S and ε_v, b) differential layer of thickness $d\omega'$, c) continuously varying swelling strain.

3. Water profiles below crack surfaces

3.1 Results by Lechenault et al. [9]

Subcritical crack growth tests were carried out on DCDC specimens of silica by Lechenault et al. [9]. The water entrance into the fracture surfaces formed by the passage of the crack exposed to deuterium oxide D_2O was evaluated with a <u>neutron reflection technique</u> to measure the penetration of the deuterium oxide into the silica glass. The authors found a satisfactory fit to the reflection data by assuming that the water concentration was constant at the surface up to a distance of L, followed by an exponential decrease in concentration for distances greater than L.

Consequently, Lechenault et al. [9] fitted their results by the expression

$$C_w/C_w(0) = \begin{cases} 1 & \text{for} \quad z \leq L \\ \exp[-(z-L)/\eta] & \text{for} \quad z > L \end{cases} \tag{15}$$

and found the parameters L=4.3 nm, η=3.5 nm for a region of low crack rates ($v \approx 10^{-8}$ m/s) at K= 0.61 MPa·m$^{1/2}$ and L=4.6 nm, η=2.3 nm for higher crack rates ($v \approx 4 \; 10^{-6}$ m/s) at K= 0.77 MPa·m$^{1/2}$. These water profiles are illustrated in Fig. 4.
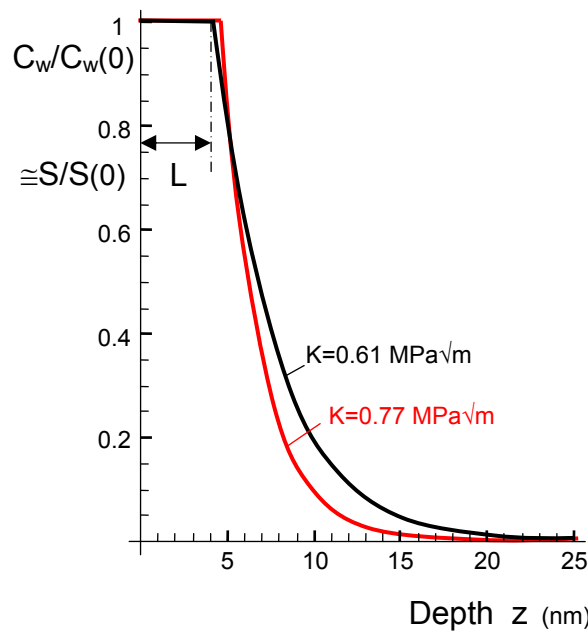
Fig. 4 Normalized water profiles measured by Lechenault et al. [9] on DCDC specimens fractured in heavy water, $C_w(0)$ = concentration at the surface.

3.2 Result by Tomozawa et al. [10]

The concentration of water below the crack surfaces was measured by Tomozawa et al. [10] using the <u>nuclear reaction analysis</u> (NRA). The profile of the hydrogen concen-

5

tration is shown in Fig. 5a. In order to allow an approximate extrapolation of measured data to the surface, we fitted the data c_H by a complementary error function

$$c_H = c_{H,0}\, \text{erfc}\left[\frac{z}{2b}\right] + \underbrace{0.005 \times 10^{22}\,/\,\text{cm}^3}_{\text{Background}} \tag{16}$$

taking into account the background level of 0.005 10^{22}/cm^3. The coefficient $c_{H,0}$ is the surface concentration.

The red bar in Fig. 5a indicates the 90%-CI of the surface concentration. The depth b at which the concentration decreased to $\cong 50\%$ of the surface value in Fig. 5a is about 5 nm. By fitting (16) to the measurements, the best set of parameters was from [11] is

$$c_{H,0} = 1.30\,[1.055, 1.55]\,10^{22}/\text{cm}^3,\ b = 4.95\,[3.28, 6.61]\,\text{nm}^{-1}\ (90\%\ \text{CI}).$$

with the mean squares sum of 11.65 $(10^{22}/\text{cm}^3)^2$.

The maximum hydroxyl concentration at $z=0$, $S(0)$, could be computed in [11] with the result

$$S(0) = 16.5[14.4, 18.4]\ (\text{wt}\%) \tag{17}$$

For a second description of the water distribution let us be guided by the results of Lechenault et al. [9]. We fitted the measurements by Tomozawa et al. [10] also via eq.(15) with the parameters

$$c_{H,0} = 1.12\,10^{22}/\text{cm}^3,\ L = 3.0\,\text{nm},\ \eta = 2.96\,\text{nm}$$

and a mean squares sum of $11.78 \times (10^{22}/\text{cm}^3)^2$.

The result is shown in Fig. 5b. Having in mind the rather strong scatter of the surface values, the two representations in Figs. 5a and 5b are equal.

4. Computation of shielding stress intensity factors

4.1 Evaluation for undamaged material

Subtracting the background level and introducing eq.(16) into eq.(13) results in

$$K_{sh} = \int_0^\infty \kappa\, S(\omega')\, h(\omega')\, d\omega' = -\psi\sqrt{2/\pi}\,\frac{\kappa S(0)E}{1-\nu}\sqrt{b}\,\Gamma(\tfrac{3}{4}) \tag{18}$$

with the Euler Gamma function Γ that for the argument ¾ reads $\Gamma(3/4) = 1.2254$, so that we can finally write with $\sqrt{2/\pi}\,\Gamma(3/4) = 0.9777 \cong 1$

$$K_{sh} \cong -\psi\,\frac{\kappa S(0)E}{1-\nu}\sqrt{b} \tag{19}$$

Comparison of eqs.(9) and (19) allows to identify approximately: $b \cong \omega$. For the representation of the water profile by eq.(15), introducing into eq.(13) yields

6

$$K_{sh} = \int_0^\infty \kappa S(\omega') h(\omega') d\omega' = -\psi \frac{\kappa S(0) E}{1-v} \left(\sqrt{L} + \frac{1}{2} \sqrt{\pi \eta} \exp\left(\sqrt{\frac{L}{\eta}} \right) \mathrm{erfc}\left(\sqrt{\frac{L}{\eta}} \right) \right) \qquad (20)$$

From the surface concentration in Fig. 5a, given by eq.(17), the shielding stress intensity factor results as

$$K_{sh} \cong -0.21 \; \mathrm{MPa}\sqrt{m} \qquad (21)$$

For the description by eq.(15) we obtain:

$$K_{sh} \cong -0.20 \; \mathrm{MPa}\sqrt{m} \qquad (22)$$

where $\cong 73\%$ of the total value come from the constant part of the water profile.
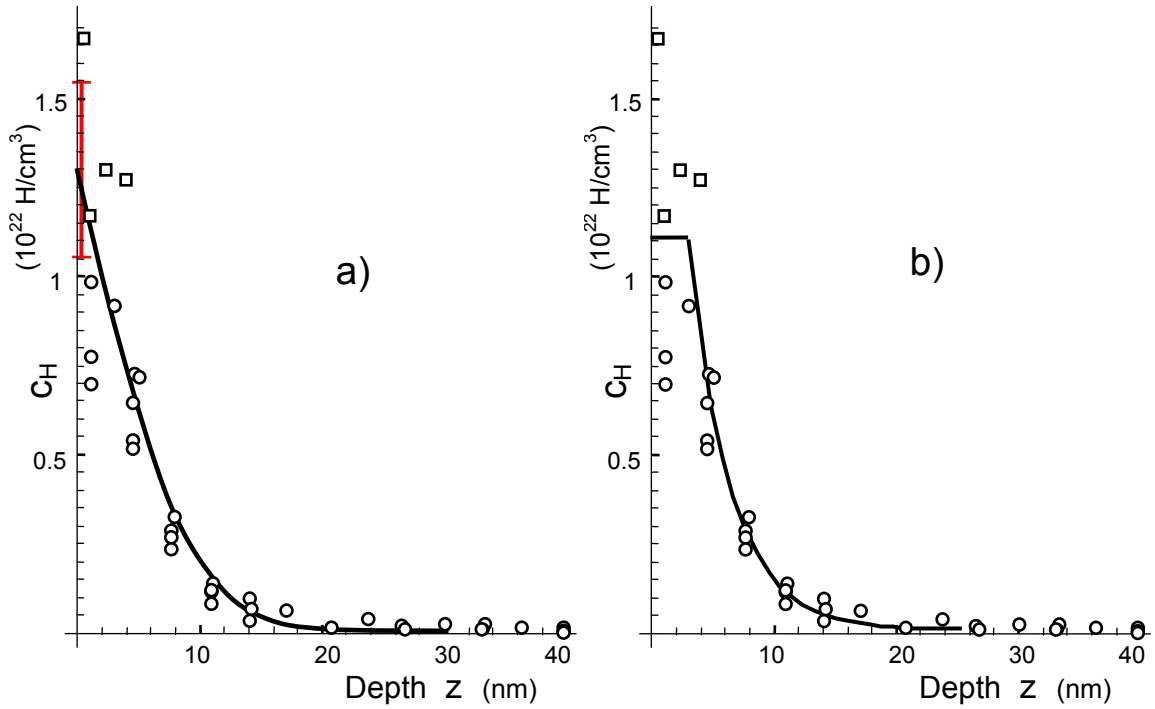
Fig. 5 Hydrogen concentration in the surface region of a growing crack via NRA-measurements by Tomozawa et al. [10], a) representation by eq.(16), b) expressed via eq.(15).

4.2 Evaluation for damaged material

The hydroxyl concentration in the crack-tip region causes damage since the originally intact silica ring structure is cracked by the water attack. One of the consequences of such damage is the reduction of Young's modulus E. In order to describe this E-decrease, we used in [12] the rather simple damage model proposed by Phany and Niyogi [13]. When E_D is the modulus in the damaged state and E_0 the value for undamaged silica, we could derive the relation [12]

$$\frac{E_D}{E_0} = (1 - \gamma S)^2 = (1 - S / S_{max})^2 \tag{23}$$

with $\gamma=5.3$ [4.35, 6.25] (90%-CI in brackets). The related dependency is shown in Fig. 6. The hydroxyl concentration at which the Young's modulus disappears at $S_{max}=1/\gamma= 0.188$ [0.16, 0.23].
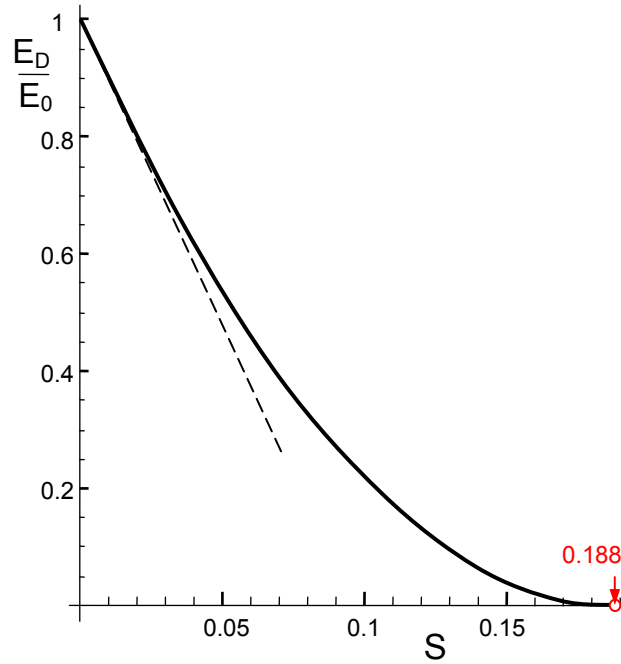
Fig. 6 Effect of hydroxyl concentration on Young's modulus according to eq.(23).

Including the varying modulus into the computation of the shielding stress intensity factor requires a modification of eq.(13). Now the stress intensity factor results from

$$K_{sh} = \frac{1}{E_0} \int_0^\infty (S \times E) h(\omega') \, d\omega' \tag{24}$$

The product $S \times E$ that governs the shielding stress intensity factor according to eq.(24) is shown in Fig. 7a. The blue curve shows the result for the representation by eq.(16) and the red curve by eq.(15). The region at a depth of $z \approx 5\text{-}6$ nm has the strongest influence on shielding. Figure 7b gives the shielding stress intensity factor as a function of the maximum hydroxyl concentration at the surface.

From this diagram it results clearly lower shielding effect than for undamaged silica, namely for

distribution Fig. 5a: $\quad\quad\quad\quad K_{sh}=-0.034$ MPa√m $\tag{25}$

distribution Fig. 5b: $\quad\quad\quad\quad K_{sh}=-0.030$ MPa√m $\tag{26}$

In the latter case, the shielding stress intensity factor can be computed analytically. It results with the integral

$$I_n = \int_L^\infty \exp\left[-n\frac{(z-L)}{\eta}\right]\frac{1}{\sqrt{z}}\,dz = \sqrt{\frac{\pi\eta}{n}}\exp\left[\frac{nL}{\eta}\right]\mathrm{erfc}\left[\sqrt{\frac{nL}{\eta}}\right] \quad (27)$$

$$K_{sh} \cong -\psi\frac{\kappa E_0 S(0)}{2(1-\nu)}\left(2(1-\gamma S(0))^2\sqrt{L}+I_1-2\gamma S(0)I_2+\gamma^2 S(0)^2 I_3\right) \quad (28)$$
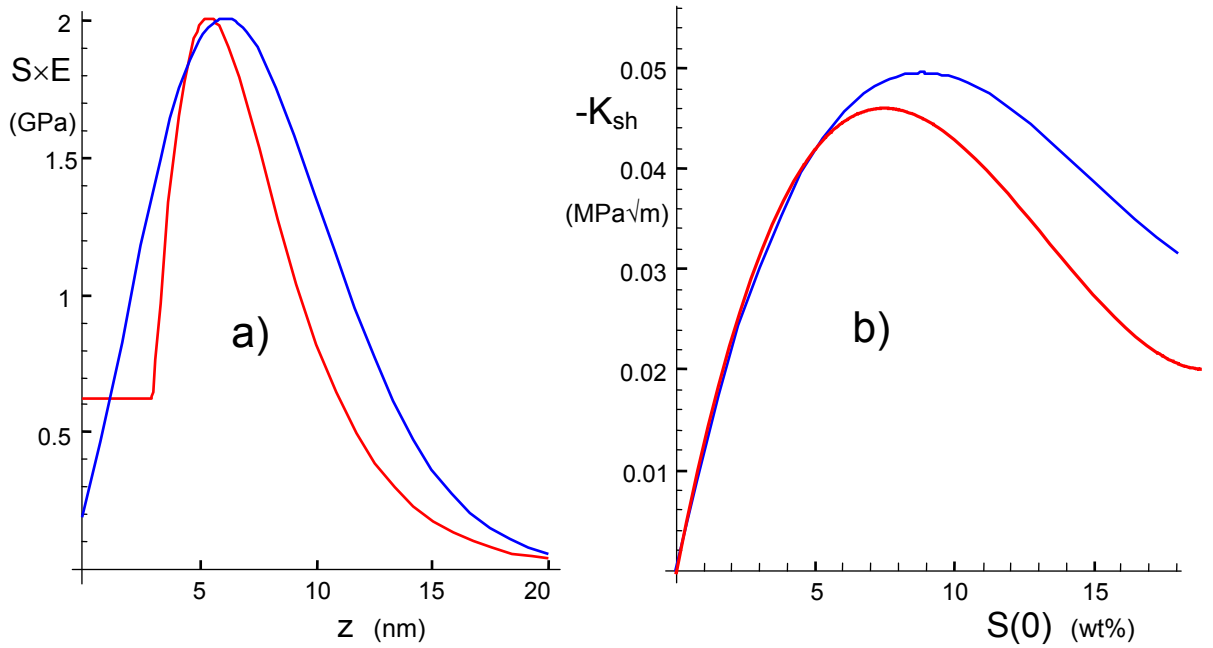
Fig. 7 a) Distribution of the product $S\times E$ relevant for eq.(24), b) shielding stress intensity factors for the representations by eq.(15) (red curve) and eq.(17) (blue curve).

The concentration profiles by Lechenault et al. [9], Fig. 4, clearly show the characteristic shape with a plateau as would be expected from the Irwin and Dugdale crack-tip zone models for "plastic flow" behaviour. An interpretation by the Irwin model will be given in a separate report.

4.3 Shielding stress intensity factor in the unloaded state

In the case of disappearing total stress intensity factor at the crack tip, $K_{total}=K_{appl}+K_{tip}$ ≤0, all volume elements in the water-affected zone are under compression due to volume swelling by hydroxyl generation [8]. In the previous considerations, we applied the model of pore-like defects. This model describes symmetrical material response under tension and compression loading. The Young's modulus in compression is not necessarily identical in tension and compression. This problem was handled by

Lemaitre and Sermage [14] introducing non-symmetry of deformation in tension and compression. These authors included the case that the reduction of Young's modulus in compression is less strong than in tension by a non-symmetry coefficient or crack closure parameter $0 \leq \alpha \leq 1$

$$E = \begin{cases} E_0(1-D) & \text{for} & \sigma \geq 0 \\ E_0(1-\alpha D) & \text{for} & \sigma < 0 \end{cases} \tag{29}$$

For most practical applications Lemaitre and Sermage suggest $\alpha=0.2$ [14].
Figure 8a again shows the shielding stress intensity factor for the hydroxyl concentration according to eqs.(15) and (29) for different values of the symmetry parameter α.

5 Crack-tip shielding and threshold behaviour

When a grown crack has been unloaded and is again loaded, the crack tip will only see loading by a stress intensity factor if $K_{appl} > K_{sh}$. Consequently, the shielding stress intensity factor causes a threshold value for the subcritical crack growth as is schematically illustrated in Fig 8b. The stress intensity at which K_{total} and crack growth rate disappear in a crack-growth test under monotonously decreasing loading may be denoted as $K_{appl}(K_{tip}=0)=K_0$. Then it holds for a crack-arrest test under decreasing load

$$K_{total} = K_{appl} + K_{sh} = 0 \tag{30a}$$

or
$$K_0 = -K_{sh} \tag{30b}$$

It should be emphasized that this threshold behaviour can only occur if the cracks have already grown subcritically (Fig. 1b). Cracks that are loaded for the first time can grow immediately, since the shielding zone has a heart-shaped contour (Fig. 1a) for which $K_{sh}=0$ [3]. The shielding stress intensity K_{sh} is plotted for a zone of height ω as shown in Fig. 9 according to McMeeking and Evans [3]. Their data were simply described by Evans and Faber [15] as

$$\frac{K_{sh}}{K_\infty} = \frac{2}{\pi}\arctan(\Delta a / \omega) \tag{31}$$

Since the applied stress intensity factor for a constant applied load depends on the crack extension Δa via

$$\frac{K_{appl}}{K_{appl,0}} = \sqrt{1+\frac{\Delta a}{a_0}} = \sqrt{1+\frac{\Delta a / \omega}{a_0 / \omega}} \tag{32}$$

where $K_{appl,0}$ stands for $K_{appl,\Delta a=0}$. Whereas for a crack growing at $K_{total} > 0$, the applied stress intensity factor increases and the shielding stress intensity factor becomes

stronger negative. The total stress intensity factor must first increase and then decrease. After a minimum, the total stress intensity factor rises again.
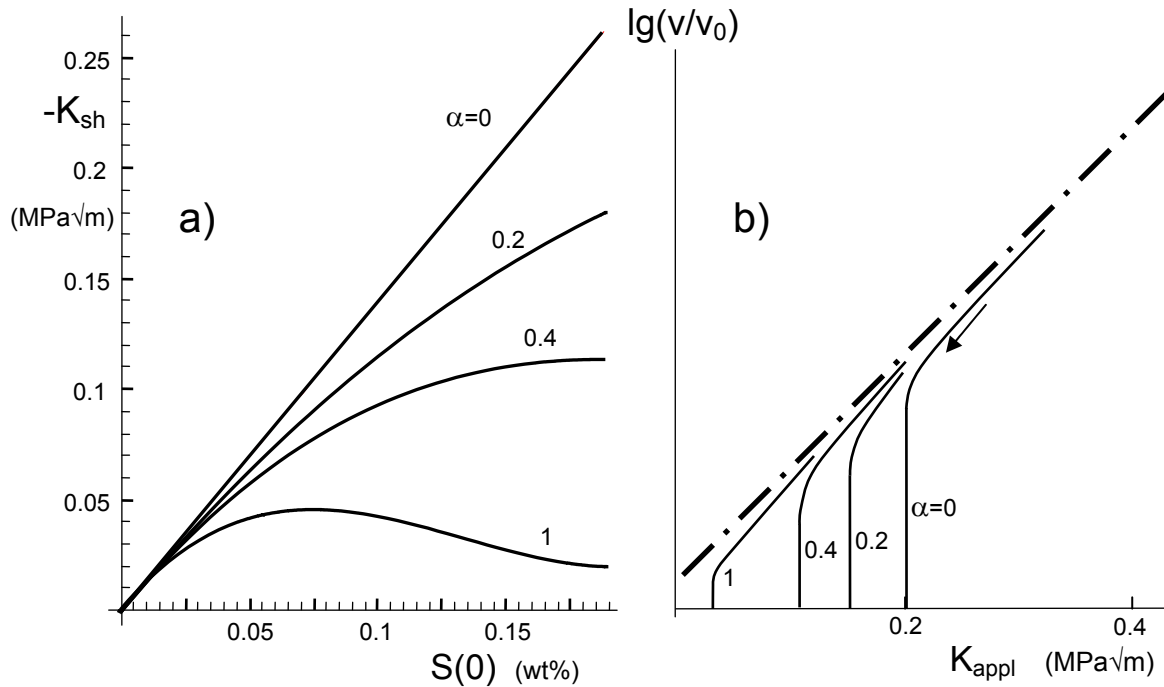
Fig. 8 a) Shielding stress intensity factors for the representations by eqs.(15) and (29) for the unloading case of $K_{total} = K_{appl} + K_{sh} < 0$, b) expected threshold values of the v-K_{appl} curve.
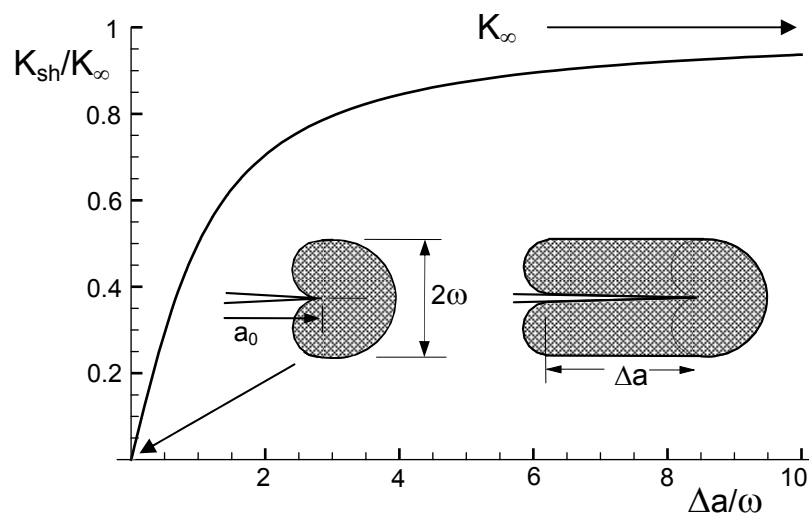
Fig. 9 Shielding stress intensity factor K_{sh} normalized on its saturation value K_∞, reached for $\Delta a/\omega \to \infty$ obtained by McMeeking and Evans [3].

The arrest condition, eq.(30a,b) is illustrated in Figs. 10a and 10b for short cracks of different initial lengths a_0/ω and varying saturation values K_∞ of the shielding stress intensity factor. The shielding stress intensity factor can depend in principle on the externally applied load and the actual crack rate. For reasons of transparency we

11

assume in Figs. 10a and 10b constant values for ω and K_∞. Crack arrest occurs in those cases for which the curves intersect the line $K_{total}=0$, indicated by the open circles. The dashed extensions are hypothetic total stress intensity factors which make no physical sense since stress singularities at a crack tip are only present for $K_{total}>0$. From Fig. 10b it becomes obvious that subcritical crack growth for small cracks can take place below that threshold stress intensity factor that occurs in the case of cracks under decreasing loading (here $K_0=0.2$ MPa$\sqrt{m}$).
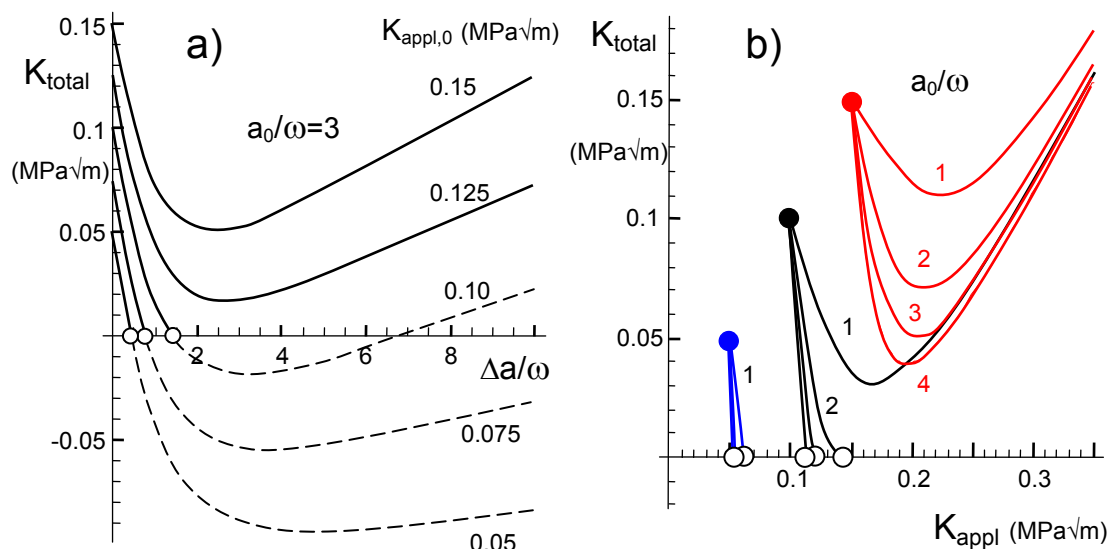
Fig. 10 Total stress intensity factor for $K_\infty = -0.2$ MPa$\sqrt{m}$, open circles: arrest condition $K_{total}=0$; a) K_{total} vs. Δa for $a_0=3\omega$, b) K_{total} vs. K_{appl} for different initial crack lengths a_0.

References

1 H. Le Chatelier, *C.R. Acad. Sci. Paris* **99**(1884), 786.

2 Shelby, J.E., "Density of vitreous silica," J. Non-Cryst. **349** (2004), 331-336.

3 McMeeking, R.M., Evans, A.G., Mechanics of Transformation-Toughening in Brittle Materials, J. Am. Ceram. Soc. **65**(1982), 242-246.

4 G. Rizzi, T. Fett, Defects at silica surfaces and crack-tip shielding- A Finite Element Study, **33**, 2015, ISSN: 2194-1629, Karlsruhe, KIT.

5 Zhao, T., Nehorai, A., Detection and localization of a moving biochemical source in a semi-infinite medium, Report, Electrical and Computer Engineering Dept. Univ. of Illinois, Chicago, USA.

6 Babich, V.M., On asymptotic solutions of the problems of moving sources of diffusion and oscillations, UDC 534.231.1, 517.226, 1991, pp. 3067-3071, Plenum Publishing Corp.

7 T. Fett, New contributions to R-curves and bridging stresses – Applications of weight functions, IAM 3, KIT Scientific Publishing, 2012, Karlsruhe.

8 S. M. Wiederhorn, T. Fett, G. Rizzi, M. J. Hoffmann, J.-P. Guin, The Effect of Water Penetration on Crack Growth in Silica Glass, Engng. Fract. Mech. **100**(2013), 3-16.

9 F. Lechenault, D.L. Rountree, F. Cousin, J.-P Bouchaud, L. Ponson and E. Bouchaud, "Evidence of Deep Water Penetration in Silica during Stress Corrosion Fracture," Phys. Rev. Let. **106**(2011), 165504.

10 M. Tomozawa, W.-T. Han and W.A. Lanford, "Water Entry into Silica Glass during Slow Crack Growth," J. Am. Ceram. Soc. **74** [10] (1991) 2573-2576.

11 G. Schell, G. Rizzi, T. Fett, Hydroxyl concentrations on crack surfaces from measurements by Tomozawa, Han and Lanford, **82**, 2018, ISSN: 2194-1629, Karlsruhe, KIT.

12 T. Fett, G. Schell, C. Bucharsky, Hydroxyl Damage in Silica: Full-range description including large damages **126**, 2019, ISSN: 2194-1629, Karlsruhe, KIT.

13 Phani, K.H. Niyogi, K. De, Young's modulus of porous brittle solids, J. Mater. Sci. **22**(1987), 257–263.

14 J. Lemaitre, J.P. Sermage, One damage law for different mechanisms, Comp. Mech., **20**(1997), 84-88.

15 Evans, A.G., Faber, K.T., Crack-growth resistance of microcracking brittle materials, J. Am. Ceram. Soc. **67**(1984), 255-260.

www.kit.edu